



# Aluminum(III) induced green luminescence for naked eye detection: Experimental and computational studies



Sisir Lohar<sup>a</sup>, Animesh Sahana<sup>a</sup>, Arnab Banerjee<sup>a</sup>, Amarnath Chattopadhyay<sup>b</sup>, Subhra Kanti Mukhopadhyay<sup>b</sup>, Jesús Sanmartín Matalobos<sup>c,\*</sup>, Debasis Das<sup>a,\*</sup>

<sup>a</sup> Department of Chemistry, The University of Burdwan, Burdwan 713104, West Bengal, India

<sup>b</sup> Department of Microbiology, The University of Burdwan, Burdwan, West Bengal, India

<sup>c</sup> Departamento de Química Inorgánica, Facultad de Química, Avda. Das Ciencias s/n, 15782 Santiago de Compostela, Spain

## ARTICLE INFO

### Article history:

Received 2 July 2013

Received in revised form 28 November 2013

Accepted 30 November 2013

Available online 16 December 2013

### Keywords:

Luminescence

Aluminum(III)

Naked eye detection

DFT and TD-DFT studies

## ABSTRACT

Al(III) has extensive use in modern day life, however excess Al(III) can induce several health hazards, leading to Alzheimer's or Parkinson's diseases. So, easy determination of Al(III) in biological samples is highly relevant. A group of three probes, (4E)-4-(2-hydroxybenzylideneamino)-1,2-dihydro-2,3-dimethyl-1-phenylpyrazol-5-one (**APSAL**), 2-((Z)-(quinolin-8-ylimino)methyl) phenol (**AQSAL**) and (4E)-4-((2-hydroxynaphthalen-1-yl)methyleneamino)-1,2-dihydro-2,3-dimethyl-1-phenylpyrazol-5-one (**HNAP**) have been used to discriminate Al<sup>3+</sup> from other biologically relevant and common metal ions at physiological pH. Although the synthesis of **APSAL** and **HNAP** have been reported earlier, their interaction with Al<sup>3+</sup> have not been studied earlier. Interestingly, in presence of Al<sup>3+</sup>, **HNAP** generates green luminescence, which has been highly useful for its naked eye detection while the other two generate pale yellow coloration having no luminescence. The binding constant ( $6.4 \times 10^4 \text{ M}^{-1/2}$ ) and lowest detection limit ( $1.8 \times 10^{-8} \text{ M}$ ) of **HNAP** for Al<sup>3+</sup> are higher than the rest two in the series. The higher Al<sup>3+</sup> detection efficiency of **HNAP** has been rationalised from DFT and TD-DFT studies. The HOMO–LUMO energy gap reduces to the maximum extent in **HNAP**–Al<sup>3+</sup> complex compared to free **HNAP** in the series.

© 2013 Elsevier B.V. All rights reserved.

## 1. Introduction

Metal ion selective sensors have found significant importance in chemical, biological, and environmental processes [1–3]. Very recently, several fluorescent assays have been successfully developed for biological applications [4–7]. Aluminum, the third abundant element in the lithosphere is extensively used in modern life, viz. food packaging, cookware, drinking water supplies, antiperspirants, deodorants, bleached flour, antacids as well as manufacturing of cars and computers [8–10]. Excess aluminum, however, can induce several health hazards leading to Alzheimer's [11] and Parkinson's diseases [12]. Therefore, determination of Al<sup>3+</sup> in environmental and biological samples has immense importance for human health. Recently, several Al<sup>3+</sup> sensors have been reported [13–17], including some quinoline based sensors [18]. However, naked eye luminescence detection of Al<sup>3+</sup> is still rare [19]. We are actively engaged to develop low cost improved methodology for easy determination of Al<sup>3+</sup> using selective fluorescent and colorimetric probes [20]. Herein, we have systematically studied three new Al<sup>3+</sup> selective fluorescent probes by engineering their

structural variations to achieve trace level naked eye detection. Two of them have been synthesized by condensing salicylaldehyde with 4-aminoantipyrine (**APSAL**) [21] and 8-aminoquinoline separately (**AQSAL**) while the third one using 2-hydroxy-1-naphthaldehyde and 4-aminoantipyrine (**HNAP**) [22]. Studies on the already reported probe, obtained by condensing 2-hydroxy-1-naphthaldehyde with 8-aminoquinoline (**HNAQ**) is excluded [23]. All three probes can selectively discriminate Al<sup>3+</sup> from other common and biologically relevant metal ions. In presence of Al<sup>3+</sup>, emission wavelength of **APSAL** and **HNAP** undergo blue shift while **HNAP** shows green luminescence, useful for naked eye detection. Due to presence of hydrophilic –OH functionality, all the probes operate in aqueous medium enabling intracellular Al<sup>3+</sup> imaging.

## 2. Results and discussion

The proton has always acted as a significant competitor of the metal ion, so pH optimization is necessary to figure out the maximum efficiency of the probe for Al(III). Figs. S1–S3 (Supporting information, henceforth ESI) clearly demonstrate that pH 7.0 to 8.5 is suitable for the entire study. Emission intensity of **APSAL**, **AQSAL** and **HNAP** remain nearly unchanged upon addition of Al<sup>3+</sup> at pH below 4.5. At lower pH, protonation of the hydroxyl

\* Corresponding authors. Tel.: +91 342 2533913; fax: +91 342 2530452 (D. Das).  
E-mail address: ddas100in@yahoo.com (D. Das).

group may reduce its  $\text{Al}^{3+}$  binding ability whereas at alkaline pH, precipitation of  $\text{Al}(\text{OH})_3$  occurs. This is reflected in our experiments where we have observed the maximum emission intensity at pH ranging 7.0–8.5. Therefore, entire studies have been carried out in HEPES buffer solution at pH 7.4. Figs. S4–S6 (ESI) give the absorption, excitation and emission spectra of **APSAL**, **AQSAL** and **HNAP**. All three probes can selectively discriminate  $\text{Al}^{3+}$  from other common and biologically relevant metal ions such as  $\text{Mg}^{2+}$ ,  $\text{Zn}^{2+}$ ,  $\text{Cd}^{2+}$ ,  $\text{Fe}^{2+}$ ,  $\text{Cr}^{3+}$ ,  $\text{Hg}^{2+}$ ,  $\text{Mn}^{2+}$ ,  $\text{Cu}^{2+}$ ,  $\text{Fe}^{3+}$ ,  $\text{Co}^{2+}$ ,  $\text{Pb}^{2+}$  and  $\text{Ni}^{2+}$ . The emission spectrum of **APSAL** ( $\lambda_{\text{ex}} = 350 \text{ nm}$ ,  $\lambda_{\text{em}} = 505 \text{ nm}$ ) undergoes 34 nm blue shift to 471 nm in presence of  $\text{Al}^{3+}$  and increases gradually with increasing  $\text{Al}^{3+}$  concentration (quantum yield changes from  $0.016 \pm 0.001$  to  $0.061 \pm 0.002$ ) (Fig. S7, ESI). For other cations, this phenomenon is not observed (Fig. S8, ESI). Job's plot (Fig. S9, ESI) shows the probe to  $\text{Al}(\text{III})$  stoichiometry as 2:1 for the  $[\text{APSAL}-\text{Al}^{3+}]$  complex, also corroborated from its ESI-TOF MS(+) mass spectrum (Fig. S10).

The emission spectrum of **AQSAL** ( $\lambda_{\text{ex}} = 330 \text{ nm}$ ,  $\lambda_{\text{em}} = 450 \text{ nm}$ ) shows a shoulder at 380 nm, in addition to the principal emission peak, both of which increases upon gradual addition of  $\text{Al}^{3+}$  (quantum yield changes from  $0.010 \pm 0.001$  to  $0.057 \pm 0.001$ ) (Fig. S11). Other common cations (Fig. S12) failed to do so. The composition of the  $[\text{AQSAL}-\text{Al}^{3+}]$  complex is 2:1 (**AQSAL**:  $\text{Al}^{3+}$ , Fig. S13). ESI-TOF MS (+) data of the adduct (Fig. S14) supports the composition.

In presence of  $\text{Al}^{3+}$ , the emission peak of **HNAP** ( $\lambda_{\text{ex}} = 380 \text{ nm}$ ,  $\lambda_{\text{em}} = 510 \text{ nm}$ ) undergoes 49 nm blue shift, the intensity of which gradually increases with increasing  $\text{Al}^{3+}$  concentration (quantum yield changes from 0.013 to 0.09) (Fig. 1). This blue shift of the emission band is not observed with other cations (Fig. S15, ESI). Job's plot (Fig. S16, ESI) and ESI-TOF MS (+) data (Fig. S17, ESI) indicate 2:1 stoichiometry of the  $[\text{HNAP}-\text{Al}^{3+}]$  complex.

The detection limits are estimated from the fluorescence titration data based on a reported and broadly used method [24,25]. The fluorescence titration experiment for **APSAL** (at 471 nm), **AQSAL** (450 nm) and **HNAP** (at 461 nm) have been normalized between the minimum (0.0 equivalent  $\text{Al}^{3+}$ ) and the maximum intensities. A linear regression curve is then fitted to the normalized fluorescence intensity data, and the point at which the line crosses the ordinate axis corresponds to its detection limit.

**APSAL**, **AQSAL** and **HNAP** can detect as low as  $5 \times 10^{-7} \text{ M}$ ,  $5.8 \times 10^{-7} \text{ M}$  and  $1.8 \times 10^{-8} \text{ M}$   $\text{Al}^{3+}$  (Figs. S18–S20, ESI). Chelation of the probes with  $\text{Al}^{3+}$  inhibits the *cis-trans* inter-conversion by

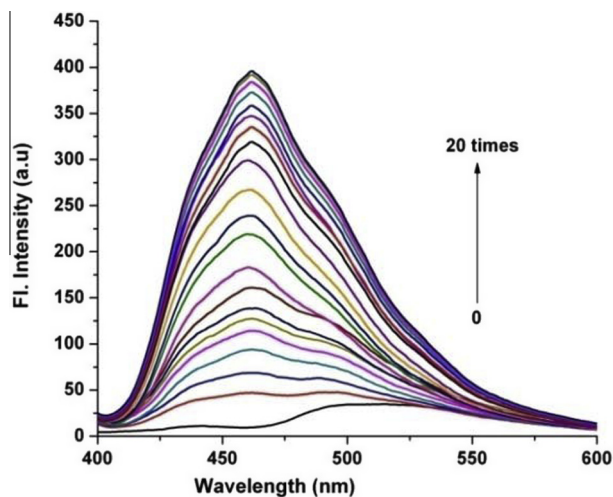


Fig. 1. Fluorescence spectral changes of **HNAP** (10  $\mu\text{M}$ ) in HEPES buffered (0.1 M) solution (methanol/water = 3:7, v/v, pH 7.4). Upon addition of different concentration of  $\text{Al}^{3+}$  (bottom:  $[\text{Al}^{3+}] = 0$ , top:  $[\text{Al}^{3+}] = 200 \mu\text{M}$ ),  $\lambda_{\text{ex}} = 380 \text{ nm}$ ,  $\lambda_{\text{em}} = 461 \text{ nm}$ .

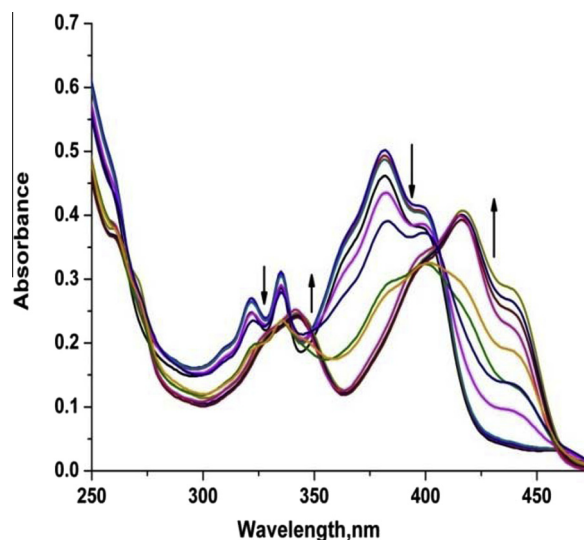


Fig. 2. Changes of absorbance of **HNAP** (10  $\mu\text{M}$ ) upon gradual addition of  $\text{Al}^{3+}$  (1, 5, 10, 15, 20, 30, 40, 50, 60, 80, 100, 150, 200  $\mu\text{M}$ ) in HEPES buffered (0.1 M) solution (methanol/water = 3/7, v/v, pH 7.4).

restricting the rotation around the  $\text{C}=\text{N}$  bond, and is responsible for fluorescence enhancement [26].

UV–Vis spectra have been recorded in HEPES buffered (0.1 M) solution (methanol/water = 3/7, v/v, pH 7.4). **APSAL** shows a peak at 346 nm along with two shoulders at 316 and 300 nm (Fig. S21, ESI). Upon addition of  $\text{Al}^{3+}$ , the absorbance at 346 nm decreases sharply while that of 316 nm increases to some extent. The intensity of a new peak that appears at 390 nm, gradually increases with increasing  $\text{Al}^{3+}$  concentration. For **AQSAL**, 335 nm peak decreases sharply with appearance of two new peaks at 271 and 413 nm (Fig. S22, ESI). **HNAP** shows peaks at 381, 334 and 321 nm (Fig. 2). In presence of  $\text{Al}^{3+}$ , the absorbance at 381 nm decreases sharply along with disappearance of two other peaks, viz. 334 and 321 nm. On the other hand, several new peaks viz. 343 and 417 nm along with two shoulders at 396 and 440 nm have appeared. All the three probes allow to detect  $\text{Al}^{3+}$  by naked eye, however,  $[\text{HNAP}-\text{Al}^{3+}]$  complex shows luminescence (Fig. 3).

The binding constants of different probes for  $\text{Al}^{3+}$  are determined using the following Benesi–Hildebrand equation [27] (Figs. S23–S25, ESI).

$$F_{\text{lim}} - F_0/F_X - F_0 = 1 + (1/K[C]^n) \quad (1)$$

where  $F_0$ ,  $F_X$ , and  $F_{\text{lim}}$  are the emission intensities of the probes in absence of  $\text{Al}^{3+}$ , at an intermediate  $\text{Al}^{3+}$  concentration, and at a concentration of complete interaction with  $\text{Al}^{3+}$  respectively.  $K$  is the binding constant,  $C$  is the concentration of  $\text{Al}^{3+}$  and  $n$  is the number of  $\text{Al}^{3+}$  ion bound per probe molecule (here,  $n = 1/2$ ). The value of  $K$ , obtained from the slope are  $1.06 \times 10^3$ ,  $8.3 \times 10^2$  and  $6.4 \times 10^4 \text{ M}^{-1/2}$  for **APSAL**, **AQSAL** and **HNAP** respectively.

Table 1 shows different photo-physical properties of the probes that allow a quick comparison.

The selectivity of different probes (**APSAL**, **AQSAL** and **HNAP**) for  $\text{Al}^{3+}$  over other common cations is examined (Figs. S26, S27, ESI and Fig. 4). No significant interference is observed. Slight interference from  $\text{Cu}^{2+}$  has been eliminated using  $\text{SCN}^-$  as masking agent. The excitation spectrum of  $\text{HNAP}-\text{Al}^{3+}$  complex lies mostly in the visible region, which might be responsible for green luminescence (Fig. S27, ESI). Fig. 5 clearly shows that the probes are easily permeable to all types of tested living cells and apparently harmless (as the cells remain alive even after a considerable time

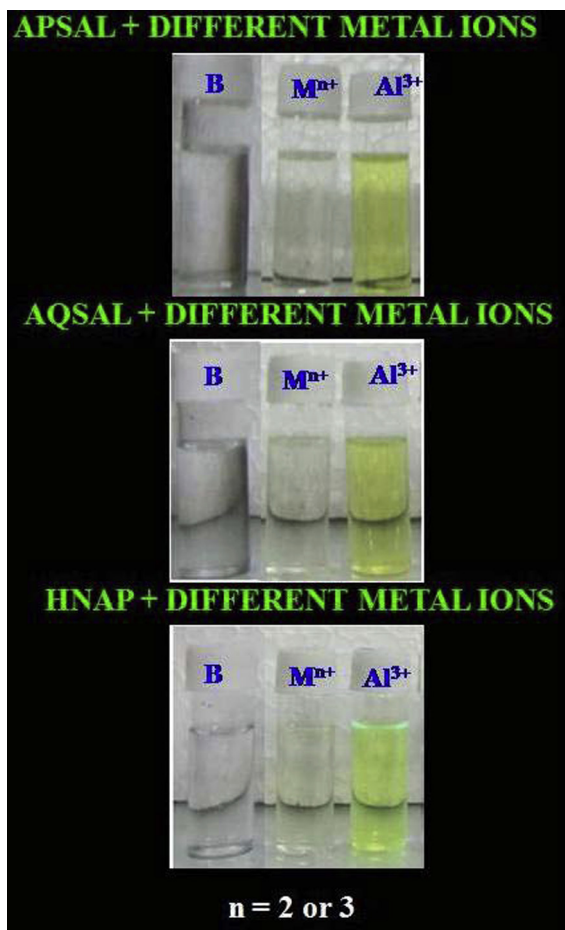


**Fig. 3.** Naked eye view of three probes (10  $\mu\text{M}$ ) in presence of different metal ions (300  $\mu\text{M}$ ).

of exposure to the probes). Thus, the probes are suitable to detect  $\text{Al}^{3+}$  ion in living cells.

### 2.1. DFT studies

Molecular level interactions between different probes with  $\text{Al}^{3+}$  have been examined using DFT method with B3LYP/ 6-31G and LanL2dZ basis set [28]. The HOMO–LUMO energy gaps in free **APSAL** and [**APSAL**– $\text{Al}^{3+}$ ] complex are 3.3763 and 3.3001 eV respectively (Fig. S28, ESI). In case of **AQSAL**, HOMO–LUMO energy gap is 3.6234 eV whereas the value for its  $\text{Al}^{3+}$  complex is 2.9475 eV (Fig. S29, ESI). On the other hand, in **HNAP** the energy gap between HOMO and LUMO is 3.5788 eV and the value reduces to 2.0057 eV for its  $\text{Al}^{3+}$  complex (Fig. 6). Thus, HOMO–LUMO energy gap is minimum in [**HNAP**– $\text{Al}^{3+}$ ] complex. With the optimized structures of the complexes, electronic transition energies are calculated by TD-DFT method. To account the effect of solvent (methanol), the conductor like polarisable continuum model (CPCM) is used. The calculated transition energies of the prominent absorption bands are shown in Tables S1–S3 (ESI) which are in close agreement with the

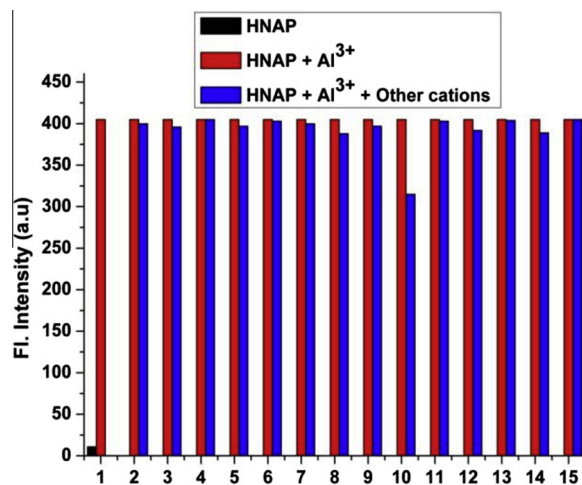


**Fig. 4.** Relative emission intensities of [**HNAP**– $\text{Al}^{3+}$ ] system in the presence of various anions in HEPES buffered (0.1 M) solution (methanol/water = 3/7, v/v, pH 7.4). Black bar: **HNAP** (10.0  $\mu\text{M}$ ). Red bar: **HNAP** (10.0  $\mu\text{M}$ ) with 30 equivalent of  $\text{Al}^{3+}$ . Blue bar: 10.0  $\mu\text{M}$  of **HNAP** and 30 equivalent of  $\text{Al}^{3+}$  with 100 equivalent of cations as stated,  $\text{Mn}^{2+}$  (2),  $\text{Co}^{2+}$  (3),  $\text{Ni}^{2+}$  (4),  $\text{Cd}^{2+}$  (5),  $\text{Hg}^{2+}$  (6),  $\text{Zn}^{2+}$  (7),  $\text{Fe}^{3+}$  (8),  $\text{Ag}^+$  (9),  $\text{Cu}^{2+}$  (10),  $\text{Na}^+$  (11),  $\text{K}^+$  (12),  $\text{Ca}^{2+}$  (13),  $\text{Mg}^{2+}$  (14),  $\text{Fe}^{3+}$  (15) ( $\lambda_{\text{ex}} = 380 \text{ nm}$ ,  $\lambda_{\text{em}} = 461 \text{ nm}$ ). (For interpretation of the references to colour in this figure legend, the reader is referred to the web version of this article.)

experimentally observed peaks as reported *supra*. The higher  $\text{Al}^{3+}$  sensing efficiency of **HNAP** relative to other two (**APSAL** and **AQSAL**) is due to the extended conjugation involving the naphthalene moiety.

## 3. Experimental

### 3.1. Materials and methods

Salicylaldehyde, 2-hydroxy-1-naphthaldehyde, 4-aminoantipyrine and 8-aminoquinoline have been used as received from Sigma Aldrich. All other chemicals and solvents are of analytical grade and used without further purification.  $\text{Al(III)}$  stock solution have been prepared from  $\text{Al}(\text{NO}_3)_3 \cdot 9\text{H}_2\text{O}$ . The sources of  $\text{Mg}^{2+}$ ,  $\text{Zn}^{2+}$ ,  $\text{Cd}^{2+}$ ,  $\text{Fe}^{2+}$ ,  $\text{Cr}^{3+}$ ,  $\text{Hg}^{2+}$ ,  $\text{Mn}^{2+}$ ,  $\text{Cu}^{2+}$ ,  $\text{Fe}^{3+}$ ,  $\text{Co}^{2+}$ ,  $\text{Pb}^{2+}$  and  $\text{Ni}^{2+}$  ions are either their chloride or nitrate salts. Absorption and emission spectra have been recorded on Shimadzu Multi Spec 1501 absorption spectrophotometer and Hitachi 4500 fluorescence spectrometer respectively. Mass spectra have been recorded in QTOF Micro YA 263 mass spectrometer in ESI positive mode. IR spectra are recorded on a Perkin Elmer FTIR spectrophotometer (model: RX-1).

### 3.2. Calculation of quantum yield

Fluorescence quantum yields ( $\phi$ ) are estimated by integrating the area under the fluorescence curves using the equation,

$$\phi_{\text{sample}} = \frac{\text{OD}_{\text{standard}} \times A_{\text{sample}}}{\text{OD}_{\text{sample}} \times A_{\text{standard}}} \times \phi_{\text{standard}}$$

where,  $A$  is the area under the fluorescence spectral curve and OD is optical density of the compound at the excitation wavelength [29].

**Table 1**  
Comparison of photo-physical properties of the three probes.

Probe name	Binding constant for $\text{Al}^{3+}$	Lowest detection limit	Detection	Stabilization energy after complexation with $\text{Al}^{3+}$	$\lambda_{\text{ex}}$ and $\lambda_{\text{em}}$
<b>APSAL</b>	$1.06 \times 10^3 \text{ M}^{-1/2}$	$5 \times 10^{-7} \text{ M}$	Yellow color generation	(3.3763–3.3001 eV) = 0.0762 eV	350 and 505 nm
<b>AQSAL</b>	$8.3 \times 10^2 \text{ M}^{-1/2}$	$5.8 \times 10^{-7} \text{ M}$	Yellow color generation	(3.6234–2.9475 eV) = 0.6759 eV	330 and 450 nm
<b>HNAP</b>	$6.4 \times 10^4 \text{ M}^{-1/2}$	$1.8 \times 10^{-8} \text{ M}$	Green luminescence	(3.5788–2.0057 eV) = 1.5731 eV	380 and 510 nm

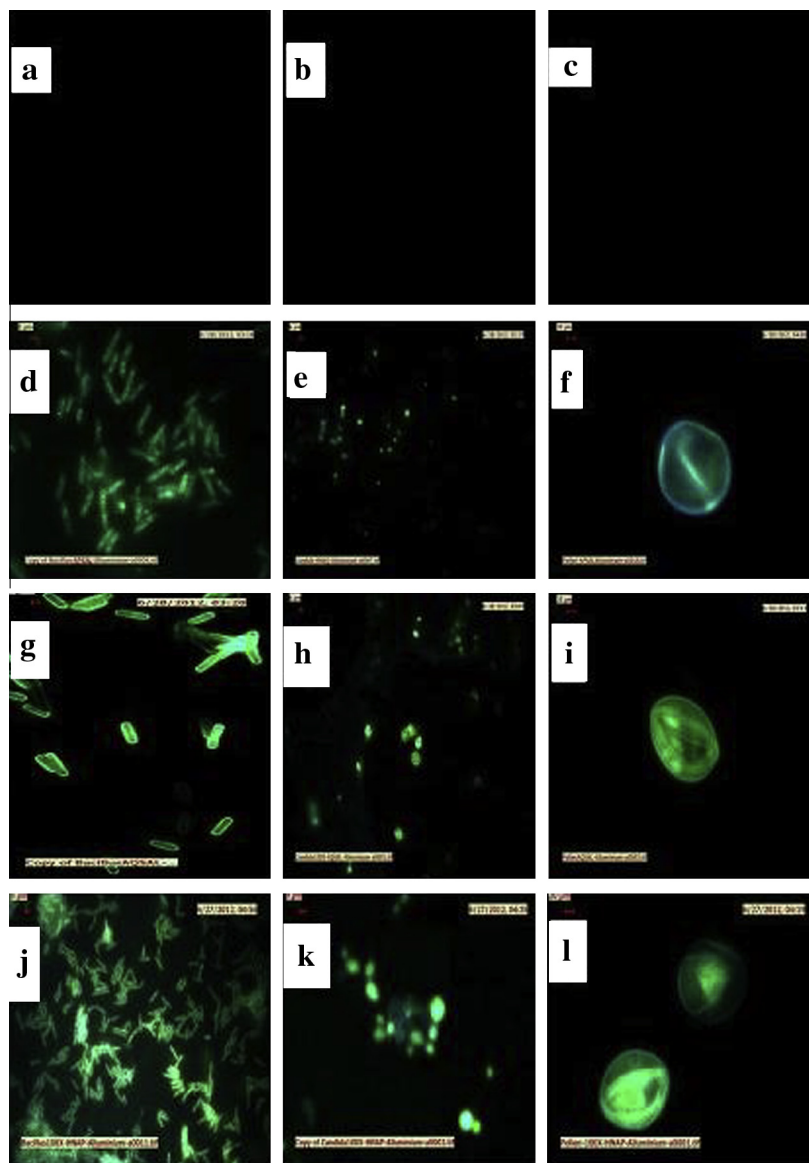


**Fig. 5.** Fluorescence images: (a), (b) and (c) are for controls, i.e. cells treated with free **APSAL**, **AQSAL** and **HNAP** respectively. Whereas images, (d), (g) and (j) are Al<sup>3+</sup> incubated *Bacillus* sp. cells after adding **APSAL**, **AQSAL** and **HNAP** respectively; Similarly, (e), (h) and (k) are the images for Al<sup>3+</sup> incubated *Candida albicans* cells after adding **APSAL**, **AQSAL** and **HNAP** respectively; (f), (i) and (l) are Al<sup>3+</sup> incubated pollen grains of *Allamandapuberula* (*Aapocynaceae*) after adding **APSAL**, **AQSAL** and **HNAP** respectively.

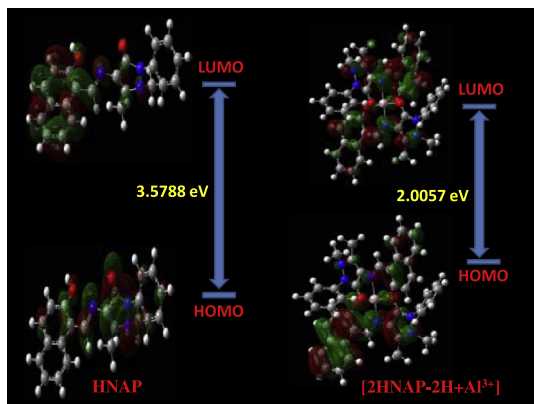
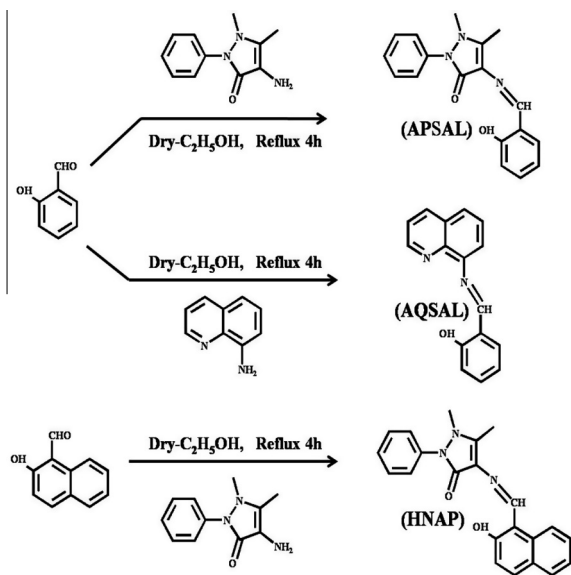


**Fig. 6.** Energy optimized structure and HOMO–LUMO energy gap of **HNAP** and its Al<sup>3+</sup> complex.

Anthracene is used as quantum yield standard (quantum yield is 0.27 in ethanol) [30] for measuring the quantum yields of **APSAL**, **AQSAL**, **HNAP** and their Al<sup>3+</sup> complexes.

### 3.3. General method of synthesis of **AQSAL**

Syntheses of **APSAL** and **HNAP** have been made as reported earlier.<sup>20,21</sup> **Scheme 1** shows the synthesis of 2-((Z)-(quinolin-8-ylimino)methyl) phenol (**AQSAL**). 8-Aminoquinoline (200 mg, 1.39 mmol) is dissolved in 20 mL dry methanol. 15 mL solution of salicylaldehyde (170 mg, 1.39 mmol) in methanol is added drop wise under stirring condition followed by refluxing for 6 h. Slow evaporation of the solvent has yielded colorless crystals of **AQSAL**. Single crystal X-ray structure of **AQSAL** is presented in **Fig. 1**. Yield, 0.31 g (90%). ESI-TOF MS (+) (**Fig. S30**, ESI): 249.08 for [L+H]<sup>+</sup> and 271.08 for [L+Na]<sup>+</sup>. <sup>1</sup>H NMR spectrum (400 MHz, CDCl<sub>3</sub>, **Fig. S31**, ESI),  $\delta$ , ppm: 14 (1H, S), 8.943 (1H, S), 8.785 (1H, d,  $J = 2.4$ ), 8.209 (1H, d,  $J = 6.4$ ), 7.735 (1H, d,  $J = 1.2$ ), 7.490 (2H, m,  $J = 4.4$ ), 7.441 (1H, m,  $J = 1.6$ ), 7.355 (1H, S), 7.184 (1H, d,  $J = 0.8$ ), 7.115 (1H, d,



**Scheme 1.** Synthesis of the probes **APSAL**, **AQSAL** and **HNAP**.

$J = 8.4$ ), 6.980 (1H, m,  $J = 6$ ). FTIR (Fig. S32, ESI): 3452 (O–H); 1618 (C=N).

#### 3.4. Synthesis of $Al^{3+}$ -probe complexes

$Al(NO_3)_3 \cdot 9H_2O$  (0.031 g, 0.082 mmol) in MeOH (10 mL) is slowly added to a magnetically stirred solution of **APSAL** (0.050 g, 0.162 mmol) in the same solvent (10 mL). The mixture is stirred for 0.5 h. ESI-TOF (+) mass (Fig. S10, ESI) spectrum for the complex shows a peak at 639.10, attributed to  $[2APSAL-2H + Al^{3+}]^+$ . Similarly,  $Al(NO_3)_3 \cdot 9H_2O$  (0.038 g, 0.1 mmol) with **AQSAL** (0.050 g, 0.2 mmol) and  $Al(NO_3)_3 \cdot 9H_2O$  (0.027 g, 0.07 mmol) with **HNAP** (0.050 g, 0.14 mmol) are mixed to obtain respective complexes. ESI-TOF (+) mass spectra (Fig. S14 and S17, ESI) show peaks at 520.93 for  $[2AQSAL-2H + Al^{3+}]^+$  and 738.96 for  $[2HNAP-2H + Al^{3+}]^+$  respectively.

Normalized excitation spectra of three complexes are presented in Fig. S33.

#### 3.5. Preparation of cells

*Candida albicans* cells (IMTECH No. 3018) are grown in yeast extract glucose broth medium (incubation temperature, 37 °C) for 24 h. It is centrifuged at 6000 rpm for 3 min and washed with normal saline. The cells are then treated with aqueous aluminum nitrate ( $1 \text{ mg mL}^{-1}$ ) solution. After incubation, cells are washed again with normal saline and observed under a fluorescence microscope equipped with UV filter after adding different probes (**APSAL**, **AQSAL** and **HNAP**). Cells incubated with different probes in absence of  $Al^{3+}$  are used as control. Similar studies with other cells viz. *Bacillus* sp. and *Allamandapuberula* (Aapocynaceae, collected from fresh pollen grains) have also been performed.

#### 3.6. Single crystal X-ray structural characterization of **AQSAL**

Single crystal X-ray diffraction studies on a colorless orthorhombic crystal obtained after slow evaporation of an ethanol solution of **AQSAL** consists of crystallographically independent molecules that comprise one quinoline unit connected by a  $-C=N-$  group to a *o*-hydroxy benzene unit. Table S4 (ESI) shows the bond distances and angles for free **AQSAL** that fall within the expected ranges. The planar conformation is stabilized through

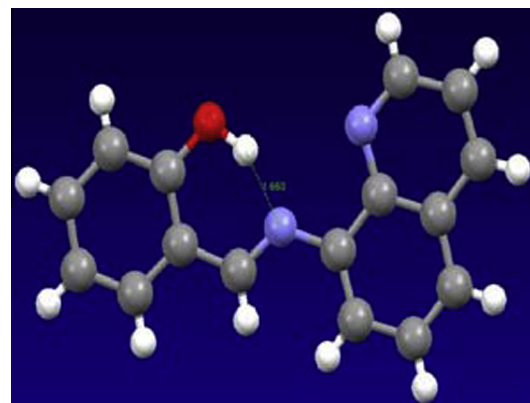


**Fig. 7.** Single crystal X-ray structure of **AQSAL**.

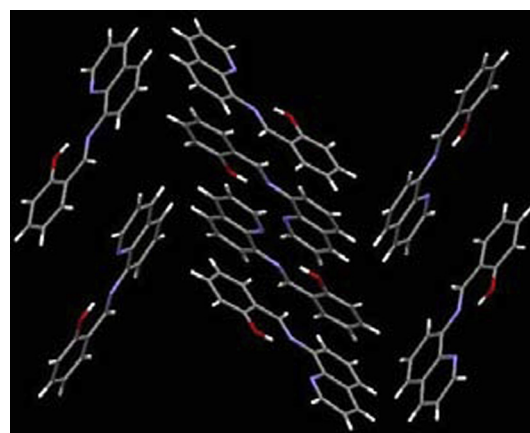


**Fig. 8.** Crystal packing of **AQSAL**.

extended conjugation and an intra-molecular H bond between O–H and N center of imine bond (Fig. 7). Moreover, molecules of **AQSAL** are perfectly stacked as evident from its crystal packing (Fig. 8).

## 4. Conclusion

In summary, **APSAL**, **AQSAL** and **HNAP** can selectively recognize  $Al^{3+}$  through CHEF mechanism. Moreover, **HNAP** shows intense green luminescence in presence of  $Al^{3+}$ , enabling its naked eye detection while the other probes generate yellow color. The excitation spectrum of **HNAP**- $Al^{3+}$  complex lies mostly in the visible region, which might be responsible for green luminescence. Binding constant of **HNAP** for  $Al^{3+}$  is nearly 10 times higher than that of two other probes. In fact, there is immense scope for the development of low cost  $Al(III)$  sensitive luminescent probes with much lower detection limit, that will function in greener solvents.

## Acknowledgements

S. Lohar and A. Sahana are grateful to CSIR, New Delhi for fellowship. Financial assistance from UGC-DAE-CSR-Kolkata is gratefully acknowledged. Authors gratefully acknowledge Indian Institute of Chemical Biology (IICB, Kolkata) for mass spectral facilities. We sincerely thank University Science Instrumentation Center (USIC), Burdwan University for fluorescence microscope facility.

## Appendix A. Supplementary material

CCDC 883038 contains the supplementary crystallographic data for this paper. These data can be obtained free of charge from The Cambridge Crystallographic Data Centre via [http://www.ccdc.cam.ac.uk/data\\_request/cif](http://www.ccdc.cam.ac.uk/data_request/cif). Supplementary data associated with this article can be found, in the online version, at <http://dx.doi.org/10.1016/j.ica.2013.11.038>.

## References

- [1] R.H. Newman, M.D. Fosbrink, J. Zhang, *Chem. Rev.* 111 (2011) 3614.
- [2] J.F. Zhang, Y. Zhou, J. Yoon, J.S. Kim, *Chem. Soc. Rev.* 40 (2011) 3416.
- [3] J. Wu, W. Liu, J. Ge, H. Zhang, P. Wang, *Chem. Soc. Rev.* 40 (2011) 3483.
- [4] (a) D. Maity, T. Govindaraju, *Inorg. Chem.* 49 (2010) 7229;  
(b) S.C. Warren-Smith, S. Heng, H. Ebendorff-Heidepriem, A.D. Abell, T.M. Monro, *Langmuir* 27 (2011) 5680.
- [5] Y. Liu, C. Deng, L. Tang, A. Qin, R. Hu, J.Z. Sun, B.Z. Tang, *J. Am. Chem. Soc.* 133 (2011) 660.
- [6] Y. Kurishita, T. Kohira, A. Ojida, I. Hamachi, *J. Am. Chem. Soc.* 132 (2010) 13290.
- [7] Z. Xu, K.H. Baek, H.N. Kim, J. Cui, X. Qian, D.R. Spring, J.Y.I. Shin, *J. Am. Chem. Soc.* 132 (2010) 601.
- [8] G.H. Robinson, *Chem. Eng. News* 81 (2003) 54.
- [9] E.R. Scerri, *The Periodic Table: Its Story and Its Significance*, Oxford University Press, 2007.
- [10] C. Exley, *J. Inorg. Biochem.* 99 (2005) 1747.
- [11] D.P. Perl, A.R. Brody, *Science* 208 (1980) 297.
- [12] D.P. Perl, D.C. Gajdusek, R.M. Garruto, R.T. Yanagihara, C.J. Gibbs, *Science* 217 (1982) 1053.
- [13] A. Sahana, A. Banerjee, S. Das, S. Lohar, D. Karak, B. Sarkar, S.K. Mukhopadhyay, A.K. Mukherjee, D. Das, *Org. Biomol. Chem.* 9 (2011) 5523.
- [14] A. Banerjee, A. Sahana, S. Das, S. Lohar, S. Guha, B. Sarkar, S.K. Mukhopadhyay, A.K. Mukherjee, D. Das, *Inorg. Chem.* 51 (2012) 5699.
- [15] S. Samanta, B. Nath, J.B. Baruah, *Inorg. Chem. Commun.* 22 (2012) 98.
- [16] S. Kim, J.Y. Noh, K.Y. Kim, J.H. Kim, H.K. Kang, S.W. Nam, S.H. Kim, S. Park, C. Kim, *J. Inorg. Chem.* 51 (2012) 3597.
- [17] Y.W. Wang, M.X. Yu, Y.H. Yu, Z.P. Bai, Z. Shen, F.Y. Li, X.Z. You, *Tetrahedron Lett.* 50 (2009) 6169.
- [18] (a) Y. Zhao, Z. Lin, H. Liao, C. Duan, Q. Meng, *Inorg. Chem. Commun.* 9 (2006) 966;  
(b) X. Jiang, B. Wang, Z. Yang, Y. Liu, T. Li, Z. Liu, *Inorg. Chem. Commun.* 14 (2011) 1224;  
(c) D. Maity, T. Govindaraju, *Chem. Commun.* 48 (2012) 1039.
- [19] D. Karak, S. Lohar, A. Sahana, S. Guha, A. Banerjee, D. Das, *Anal. Methods* 4 (2012) 1906.
- [20] (a) S. Das, D. Karak, S. Lohar, A. Banerjee, A. Sahana, D. Das, *Anal. Methods* 4 (2012) 3620;  
(b) D. Karak, S. Lohar, A. Banerjee, A. Sahana, I. Hauli, S.K. Mukhopadhyay, J.S. Matalobos, D. Das, *RSC Adv.* 2 (2012) 12447;  
(c) A. Banerjee, A. Sahana, S. Das, S. Lohar, S. Guha, B. Sarkar, S.K. Mukhopadhyay, A.K. Mukherjee, D. Das, *Analyst* 137 (2012) 2166;  
(d) S. Das, A. Sahana, A. Banerjee, S. Lohar, D.A. Safin, M.G. Babashkina, M. Bolte, Y. Garcia, I. Hauli, S.K. Mukhopadhyay, D. Das, *Dalton Trans.* 42 (2013) 4757;  
(e) A. Sahana, A. Banerjee, S. Lohar, B. Sarkar, S.K. Mukhopadhyay, D. Das, *Inorg. Chem.* 52 (2013) 3627.
- [21] S. Lohar, A. Sahana, A. Banerjee, A. Banik, S.K. Mukhopadhyay, J.S. Matalobos, D. Das, *Anal. Chem.* 85 (2013) 1778.
- [22] Z.L. You, J. Wang, J.Y. Chi, *Acta Crystallogr., Sect. E* 62 (2006) 1652.
- [23] H.M. Park, B.N. Oh, J.H. Kim, W. Qiong, I.H. Hwang, *Tetrahedron Lett.* 52 (2011) 5581.
- [24] (a) L. Wang, W. Qin, X. Tang, W. Dou, W. Liu, Q. Teng, X. Yao, *Org. Biomol. Chem.* 8 (2010) 3751;  
(b) D. Maity, T. Govindaraju, *Chem. Commun.* 46 (2010) 4499;  
(c) M. Arduini, F. Felluga, F. Mancin, P. Rossi, P. Tecilla, U. Tonellato, N. Valentinuzzi, *Chem. Commun.* (2003) 1606;  
(d) Y.W. Wang, M.X. Yu, Y.H. Yu, Z.P. Bai, Z. Shen, F.Y. Li, X.Z. You, *Tetrahedron Lett.* 50 (2009) 6169.
- [25] (a) M. Shortreed, R. Kopelman, M. Kuhn, B. Hoyland, *Anal. Chem.* 68 (1996) 1414;  
(b) A. Caballero, R. Martinez, V. Lloveras, I. Ratera, J. Vidal-Gancedo, K. Wurst, A. Tàrraga, P. Molina, J. Veciana, *J. Am. Chem. Soc.* 127 (2005) 15666.
- [26] (a) K.K. Upadhyay, A. Kumar, *Org. Biomol. Chem.* 8 (2010) 4892;  
(b) J.-S. Wu, W.-M. Liu, X.-Q. Zhuang, F. Wang, P.-F. Wang, S.-L. Tao, X.-H. Zhang, S.-K. Wu, S.-T. Lee, *Org. Lett.* 9 (2007) 33.
- [27] H.A. Benesi, J.H. Hildebrand, *J. Am. Chem. Soc.* 71 (1949) 2703.
- [28] Gaussian Inc., *Gaussian 03, Rev. C.02*, Gaussian Inc., Wallingford, CT, 2004.
- [29] E. Austin, M. Gouterman, *Bioinorg. Chem.* 9 (1978) 281.
- [30] W.H. Melhuish, *J. Phys. Chem.* 65 (1961) 229.